Type-I intermittency in semiconductor breakdown: An experimental confirmation

R. Richter, A. Kittel, G. Heinz, and G. Flätgen
Physical Institute, University of Tübingen, D-72076 Tübingen, Germany

J. Peinke
Centre de Recherche sur les Très Basses Températures, Centre National de la Recherche Scientifique, F-38042 Grenoble, France

J. Parisi
Physical Institute, University of Bayreuth, D-95440 Bayreuth, Germany
(Received 11 May 1992; revised manuscript received 16 December 1993)

Spontaneous oscillations developing during low-temperature impact ionization breakdown in extrinsic germanium are looked at with respect to characteristic features of the type-I intermittent route to chaos. We have examined the scaling behavior of the mean laminar phase length upon varying the transverse magnetic field applied. Taking into account the distribution of the phase lengths, the return map of the oscillation maxima, and the prevailing reinjection probability, we present experimental evidence that type-I intermittency takes place in a spatially extended macroscopic system with self-generated dynamics.

I. INTRODUCTION

Intermittency is a ubiquitous term that is used to characterize behavior both in space and time. The generality of the term derives from the original meaning "taking place in between" or "to send in between" of its latin root "intermittere." Therefore it suffices to have at least two clearly distinguishable, alternating states. In this way, intermittent phenomena have been studied in a wide-ranging field embracing telegraphic noise[1] as well as turbulence in pipe flows.[2]

For the class of nonlinear dissipative systems, their low-dimensional dynamics can undergo several distinct forms of intermittent behavior, namely, the three classical Pomeau-Manneville types,[3] the crisis- and the noise-induced intermittency,[4,5] and, finally, the control-parameter-caused intermittency.[6] The Pomeau-Manneville intermittent routes to chaos, classified as types I, II, and III, have in common that they obey a second-order transition. They start from a limit cycle attractor. Beyond a critical value μ_c of the relevant control parameter μ, the formerly stable periodic oscillation becomes abruptly distorted by bursts of irregular behavior. Between two successive bursts, the system returns to a regular behavior, called the laminar phase, which at a first glance looks similar to the periodic oscillation below μ_c. With increasing distance of the control parameter from the bifurcation point, $\varepsilon=\mu-\mu_c$, the bursts occur more and more frequently, and the length of the laminar phases decreases continuously. Finally, it becomes difficult at all to distinguish the two different phases. The mechanism generating this kind of continuous transition consists of a local and a global element which interact in the following manner. The local part is done by a limit cycle attractor that becomes weakly unstable via one of the three generic codimension-one bifurcations. These are the saddle node, the subcritical Neimark, and the subcritical period-doubling bifurcation.[3] The weakness of the instability is important to keep an injected trajectory for some revolutions, thus determining the average length of a laminar phase. Once the trajectory has left the weak unstable region of phase space, one needs a mechanism, called reinjection, which smashes the trajectory back to the remnant of the former attractor. This mechanism depends on the global structure of phase space. If the unstable limit cycle is embedded in a larger chaotic attractor, its dynamics gives rise to the reinjection, thus bracketing laminar with chaotic phases. Pomeau and Manneville[3] have analyzed intermittency on the basis of the local behavior of a one-dimensional iterative process derived from the Poincaré map. Under the assumption of a uniform reinjection probability, they were able to make general predictions on the scaling behavior of the mean laminar phase length $\bar{\tau}\sim\varepsilon^{\gamma}$. The exponent γ has been evaluated to $-\frac{1}{2}$ for the case of type-I intermittency, whereas for type-II and type-III intermittency γ equals -1.

Since these pioneer investigations of Pomeau and Manneville, there have been several convincing measurements on intermittency of type-I and even of the more elusive type-II and type-III transitions (see, e.g., Refs. 7, 8, and 9, respectively). However, there exist only few observations of the scaling behavior proposed. One reason is the relatively slow frequency range characteristic of most of the experimental systems established. In the case of type-I intermittency, experimental confirmation of the predicted scaling laws has been carried out mainly on the basis of analog simulations[10] and discrete electronic circuits.[11] So far, the scaling behavior of self-generated type-I intermittency has been investigated in a Taylor-Couette system.[12]

The experiment described in the following, namely, the avalanche breakdown of p-type germanium at low temperatures, represents an ideal candidate to test scalings proposed by bifurcation theory. Because of the proper time scale of semiconductor breakdown (oscillations in the kHz regime), it is easy to keep the experimental working conditions constant, necessary to verify scaling laws under variation of appropriate control parameters. Up to now, we have identified the saddle-node bifurcation on a limit cycle[13] and type-III intermittency.[14] In the present paper, we focus on the type-I intermittent transition to chaos.

The paper is organized as follows. In the next section, the experimental system together with the setup are presented. Section III covers the region of control parameter space where intermittency is observed. In Sec. IV we analyze our data with respect to peculiarities of type-I intermittency. The results are discussed in Sec. V. We also provide an explanation of some minor departures uncovered by a more careful look at the data. Our results are summarized in Sec. VI.

II. EXPERIMENT

Our experimental system consists of single-crystalline p-doped germanium, electrically driven into low-temperature avalanche breakdown via impurity impact ionization. The typical sample geometry and the electronic measuring configuration are sketched in Fig. 1. Having dimensions of about $0.2\times2\times5$ mm^3 and an acceptor concentration of about 10^{14} cm^{-3}, the extrinsic germanium crystal carries properly arranged Ohmic aluminum contacts placed on one of the two largest surfaces. To provide the outer Ohmic contacts with an electric field, a dc-bias voltage V_0 was applied to the series combination of the sample and the load resistor R_L. A dc magnetic field perpendicular to the broad sample surfaces could also be applied by a superconducting solenoid surrounding the semiconductor sample. The resulting electric current I was found from the voltage drop at the load resistor. The voltage V was measured along the sample. The inner probe contacts (of about 0.2 mm diameter) served as an independent monitor of the partial voltages V_i ($i=1,2,3$) along the sample. During the experiments, the semiconductor sample was kept at liquid-helium temperature ($T=2.1$ K) and carefully protected against external electromagnetic irradiation (visible and far infrared).

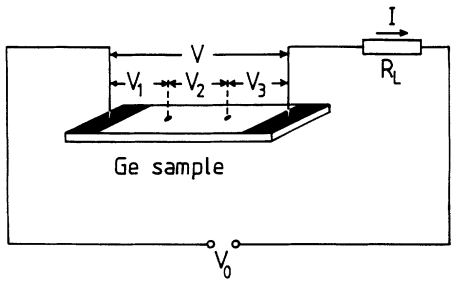

FIG. 1. Scheme of the experimental arrangement applied to the semiconductor sample. The black areas on the specimen surface indicate the Ohmic contacts.

Under these conditions, interesting nonlinear behavior emerges in the electric conductance of the semiconductor. Because of the reduced thermal energy at low temperature, the mobile charge carriers freeze out at the impurity atoms, having a binding energy of about 12 meV. Thus the material becomes highly insulating, displaying resistances in the TΩ range. If one applies a constant electric field of about 4.5 V/cm to the semiconductor, an avalanchelike multiplication of mobile charge carriers is initiated, giving rise to impurity impact ionization breakdown.[15] In the post-breakdown region, the resistance typically has a value of some 100 Ω. Such a phenomenon can be described as a nonequilibrium phase transition.[16] It is accompanied by the spontaneous formation of dissipative transport structures. Current filaments as spatial structures and current and/or voltage oscillations as temporal structures were observed in a variety of samples having different shapes of the contact and sample geometry.[17] The structure formation can be attributed to the presence of negative differential conductivity in the breakdown region. Under certain boundary conditions, a current-voltage characteristic with S-shaped negative differential resistance was found experimentally.[18]

The dynamics displays a diversity of low-dimensional nonlinear phenomena that are influenced sensitively by smallest changes of the experimental working conditions. The external magnetic field, applied in the range up to 1 T, turned out to be a convenient control parameter affecting the electric transport properties, already if varied in the μT range. We emphasize, however, that the presence of a magnetic field is not essential for observing any nonlinear behavior, in contrast to recent experimental findings for a different semiconductor system.[19] For further details of the present experiment and the underlying semiconductor physics, we refer to Refs. 20 and 21.

III. INTERMITTENCY IN PARAMETER SPACE AND PHYSICAL BACKGROUND

In the following, we demonstrate that intermittent behavior of the spontaneous oscillations is located at a certain step in the time-averaged current-voltage (I-V) characteristic. Moreover, we give some idea for the mechanism underlying the intermittent transition that derives from a destabilized filamentary structure.

Upon sweeping the bias voltage V_0 at constant load resistance $R_L=13.2$ kΩ, we found typical I-V characteristics as presented in Fig. 2 for five different values of the magnetic-field strength. Regarding the sequence (a)–(e), all characteristics clearly exhibit an S-shaped negative differential resistance in the low-current ($I\leq10$ μA) breakdown region. It has been shown elsewhere[22] in detail that such a jump results from the nucleation of the first current filament. Furthermore, the overall structure of the characteristics changes drastically. For the case of zero magnetic field [Fig. 2(a)], a hysteresis becomes obvious in the characteristic which embraces a sequence of regions of negative differential resistance. It also has been shown previously[23] that these jumps are correlated

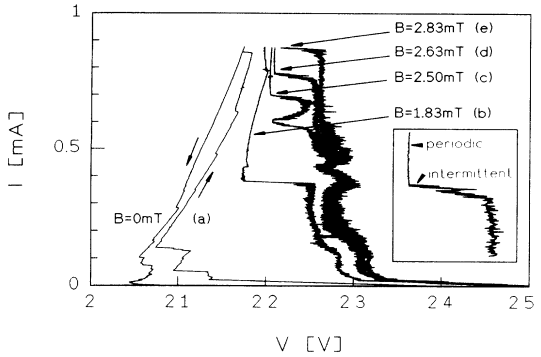

FIG. 2. Current-voltage characteristics obtained from the total sample area (see Fig. 1) at different values of the transverse magnetic field applied. The arrows along the zero-field characteristic indicate the sweep direction in the hysteretic regime. The inset displays a blowup of the step in curve (d).

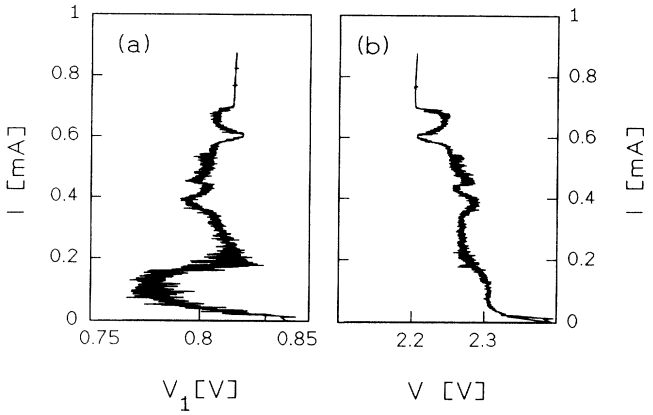

FIG. 3. Current-voltage characteristic obtained simultaneously from (a) a partial and (b) the total sample area at constant transverse magnetic field $B = 2.50$ mT.

with the nucleation of further stable current filaments. With increasing magnetic field [Fig. 2(b)], the hysteresis vanishes. Now the characteristic can be distinguished by three different parts. Immediately beyond the first jump, we recognize a noisy branch that is linked via a step to a smooth, higher-conducting branch of the characteristic. The different roughness of the smooth and noisy branches can be understood as follows. Along the smooth branch, the time trace of the voltage drop along the sample (to be discussed later on) displays stable periodic oscillations. Their period was much smaller than the averaging time constant used for measuring the *I-V* characteristic. Consequently, the high-conducting branch is smooth. On the other hand, along the noisy branch, intermittency and chaos were found. These oscillations cover time scales which partly are not averaged during the *I-V* measurement process. Hence the low-conducting branch looks noisy.

In the following, we concentrate on the step that links the lower-conducting (i.e., noisy) and the higher-conducting (i.e., smooth) branches of the characteristics in Fig. 2. Further increasing the magnetic field leads to the curves (c)–(e) where the step is shifted to higher current values. This finding can be interpreted as a destabilization of the higher-conducting branch under the influence of the transverse magnetic field. In addition, the structure of the step is modified. It becomes less steep and is covered with fluctuations. For the detailed form of the transition, e.g., on curve (d), we refer to the blowup given in the inset of Fig. 2. One edge of the step is round shaped; the other shows a sharp corner. The latter separates regions of periodic and intermittent oscillatory behavior; it marks the bifurcation point of intermittency classified as type I later on.

In Fig. 3 we juxtapose two *I-V* characteristics obtained simultaneously from (a) a partial and (b) the global voltage drop along the sample for constant magnetic field ($B = 2.63$ mT). Obviously, the curves are correlated for $I < 100$ μA, yet anticorrelated in the range $100 < I < 700$ μA. Again, focusing on the step (at $I = 700$ μA), one recognizes an increase of the partial voltage V_1 [Fig. 3(a)] during the decrease of the total voltage V [Fig. 3(b)]. Next, we give a simple explanation via analysis of the circuitry schemed in Figs. 4(a) and 4(b). For the moment, we start with a picture guided by experimental observations as shown in Figs. 4(c) and 4(d). In the periodic oscillatory state, there exists a Y-shaped filamentary structure [Fig. 4(c)], the diameter of which fluctuates (for details, see Ref. 24). On the other hand, we have a single current filament [Fig. 4(d)] in the lower-conducting, noisy state of the characteristic. Intermittency then originates from the destabilization of one branch of the Y-shaped filament, finally joining the single-filament state [Fig. 4(d)]. Back to the scheme, we discuss the development of the different voltage drops shown in Fig. 3 by the help of the circuitry. Starting from the higher-conducting state, the situation can be modeled by the resistor network of Fig. 4(a). If one lowers the bias voltage, resistor R_3 becomes more and more disconnected [Fig. 4(b)] in the time average, and the overall resistance increases. Conse-

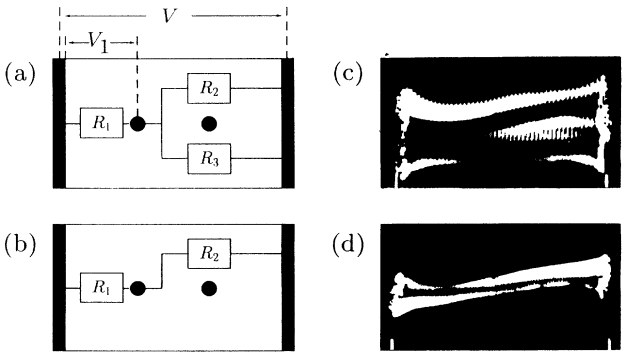

FIG. 4. (a),(b) Circuitry schemes and (c),(d) measured images of two filamentary structures: (a),(c) a Y-shaped and (b),(d) a single current filament. The images (c) and (d) are obtained from a different sample (of about 0.5 mm length) via use of low-temperature scanning electron microscopy (for details, see Refs. 23 and 24).

quently, the current I and also the partial voltage V_1 decrease, while the total voltage V increases. Further confirmation of the present simple resistor model can be provided if one compares the time traces of the voltage drops V_1 and V (not shown here). They clearly show anticorrelated dynamics.

Our interpretation of the above findings associates magnetic-field-induced intermittency with a certain regime of negative differential resistance in the I-V characteristic. We have proposed a simple model scheme aiming to spatiotemporal pattern formation of the conducting state in the semiconductor sample. For the spatially homogeneous case, a recent theoretical treatment based on the generation-recombination kinetics of hot electrons and the dynamical Hall electric field has been given elsewhere.[25]

IV. INTERMITTENT OSCILLATIONS

We now turn to the analysis of the dynamical aspects of the intermittent transition. In Fig. 5, three representative time-series records of the oscillatory behavior are plotted. In the following, we discuss oscillations of the local voltage drop V_1 as a function of the control parameter. Hereto, the transverse magnetic field was varied gradually, while keeping the bias voltage constant at $V_0 = 12.0$ V (in contrast to the I-V characteristic). Starting well above the step stressed in Fig. 2, one observes periodic oscillations as shown in Fig. 5(a). With slightly increasing magnetic field, the step shifts to higher currents until, finally, it overcomes the operating point defined by the intersection of the I-V characteristic with the load line $[I = (V_0 - V)/R_L]$. Hence the intermittent region is entered. A further increase of the control parameter leads to a chaotic state. The corresponding time traces are displayed in Figs. 5(b) and 5(c), respectively. In the following, we concentrate on the peculiarities of type-I intermittency (as summarized, e.g., in Ref. 26).

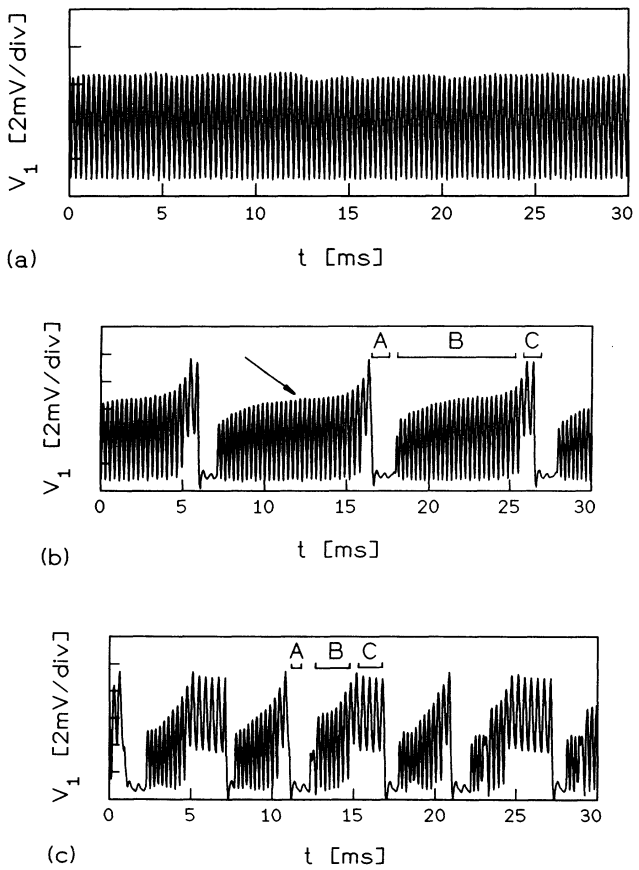

FIG. 5. Temporal structure of the partial voltage obtained at different transverse magnetic field (a) $B = 2.64$ mT, (b) $B = 2.67$ mT, (c) $B = 2.79$ mT, and the constant parameters bias voltage $V_0 = 12.00$ V, load resistance $R_L = 13.2$ kΩ, and time-averaged current $\bar{I} = 0.826$ mA. The letters A, B, and C mark different oscillatory states. For further details, see text.

We start with analyzing the time traces of Fig. 5. The oscillation shown in part (a) looks almost periodic. Small fluctuations present in the form of some low-frequency modulation of the amplitude will be the subject of a later discussion. The intermittent signal in part (b) consists of three different time patterns. A low-amplitude spiral (burst) indicated by A is followed by the laminar phase B. Before the next burst appears, we observe a few intermediate oscillations on a higher voltage level marked by C. The laminar phase displays a monotonic increase of the oscillation maxima with time. Looking more carefully at the increase of the maxima, one clearly unveils a turning point (indicated by an arrow) characteristic for a saddle-node bifurcation. Part (c) gives the fully developed chaotic dynamics. The laminar phases B become very short and almost disappear. Besides, the number of revolutions on the upper level (C) increases. A second type of laminar phase is born.

To get deeper insight into the complex time signal of Fig. 5(b), a three-dimensional attractor reconstruction (obtained via the time delay method) is presented in Fig. 6. The domains of the attractor corresponding to the different time patterns discussed above are labeled A, B, and C again. The small spiral near the origin of the axes (A) suggests the existence of a saddle focus. A two-dimensional manifold (approximately parallel to the X-Z plane) attracts the trajectories in a spiralling manner. The direction of the unstable manifold is parallel to the Y axis, thus providing a reinjection mechanism for the remnant of the formerly stable attractor (B). It is just the broad annulus in the center that generates the laminar phases with increasing amplitudes. The trajectories leaving this area enter the upper unstable cycle C before the saddle focus attracts them again. Bear in mind that the attractor comprehends several parts which are able to keep the trajectories for some regular oscillations. Hence, in a certain parameter range, intermittent time series with two coexistent laminar phases are generated [see Fig. 5(c)]. In the following, we only focus on the laminar phase B.

In order to prove that these laminar phases originate from a saddle-node bifurcation, we have determined the scaling of their mean laminar length $\bar{\tau}$. For 30 different values of the magnetic-field control parameter, each time $\bar{\tau}$ has been estimated from more than 400 phases, mea-

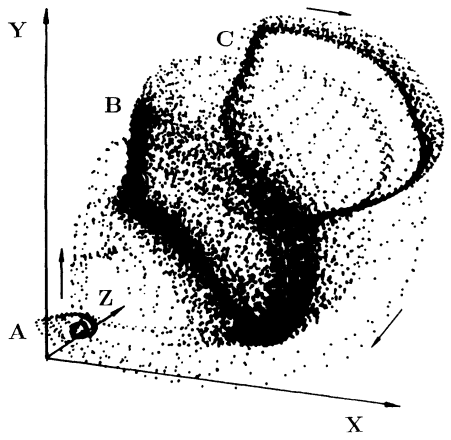

FIG. 6. Three-dimensional reconstruction of the attractor corresponding to the voltage signal of Fig. 5(b) obtained via use of the time delay method (delay 80 μs). According to Fig. 5, the letters *A*, *B*, and *C* indicate different parts of the global attractor, namely, a saddle focus (*A*), the remnant of the formerly stable core attractor (*B*), and another weak unstable limit cycle (*C*). The arrows indicate the direction of the flow on the attractor.

sured in number of revolutions. In Fig. 7, $\bar{\tau}$ is plotted as a function of the magnetic field. The experimental data are marked by solid squares. The inset clearly displays the linear scaling of the inverse square of $\bar{\tau}$ in the vicinity of the bifurcation point, just as expected for type-I intermittency.

Next, we discuss the first return maps presented in Fig. 8. Each map has been constructed from 3000 oscillation maxima out of the time signals plotted to some extent in Fig. 5. Analogously, the different domains have been labeled *A*, *B*, and *C* in Figs. 8(b) and 8(c). On the left-hand side of these two graphs, we have attached histograms displaying the distribution of reinjections. The sequence

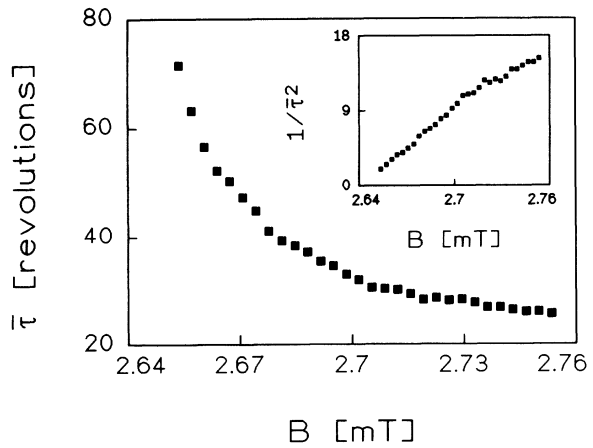

FIG. 7. Mean laminar phase length vs transverse magnetic field. To elucidate the scaling, the inverse square of the mean laminar phase length is plotted in the inset. The constant parameters are the same as in Fig. 5.

of first return maps clearly unveils the peculiarities of type-I intermittency: Under variation of the control parameter, the node in Fig. 8(a) collapses with the (invisible) saddle point. Afterwards, it disappears, leaving a long channel between the curve (domain *B*) and the first bisectrix (solid line). The motion through the channel requires a large number of iterations and gives rise to the laminar phase. Moreover, the "bottleneck" of the channel (i.e., the point of its narrowest width) reflects the turning point during the increase of the oscillation maxima, indicated

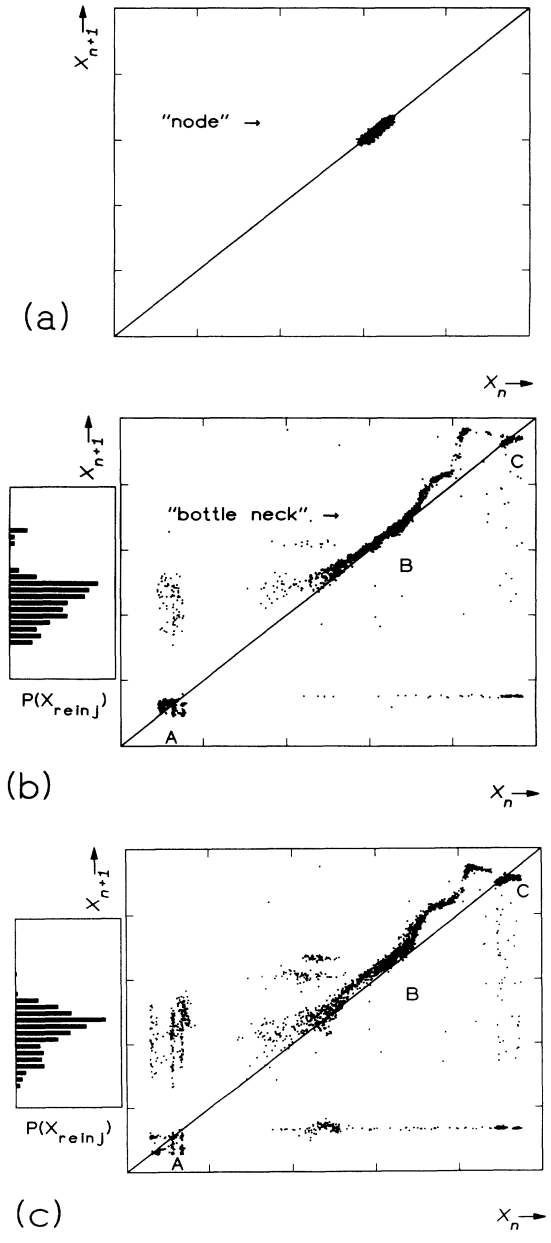

FIG. 8. Next amplitude maps of voltage signals corresponding to that of Fig. 5. According to Fig. 6, the letters *A*, *B*, and *C* indicate different parts of the global attractor. The histograms plotted in parts (b) and (c) display the reinjection probability calculated from 5000 revolutions. The vertical axes of the return map and the histogram have the identical scale.

by an arrow in the time record of Fig. 5(b). Upon further increasing the distance of the experimental control parameter from its critical value at the bifurcation point, the curve is lifted up, as indicated in Fig. 8(c). Hence the width of the channel increases, and consequently, the length of the laminar phases decreases. Thus analysis of the first return maps demonstrates that the local dynamics around the remnant of the former node can to some extent be approximated by the one-dimensional map

$$x_{n+1}=x_n+x_n^2+\varepsilon\ , \tag{1}$$

with $\varepsilon=\mu-\mu_c$.[3]

The return maps of Fig. 8 exhibit two further interesting aspects. First, the periodic structures apparent in the iterative dynamics at low values of x_n (indicated by A) together with the saddle focus in region A of Fig. 6 may result from Shilnikov chaos, as proposed by Arecchi *et al.*[27] Second, we recognize a further, yet short laminar channel at high values of x_n (indicated by C) situated under the first bisectrix. Consequently, it generates laminar phases with decreasing amplitude. This laminar phase is of the second type mentioned above. However, it does not belong to the type-I intermittency we analyze.

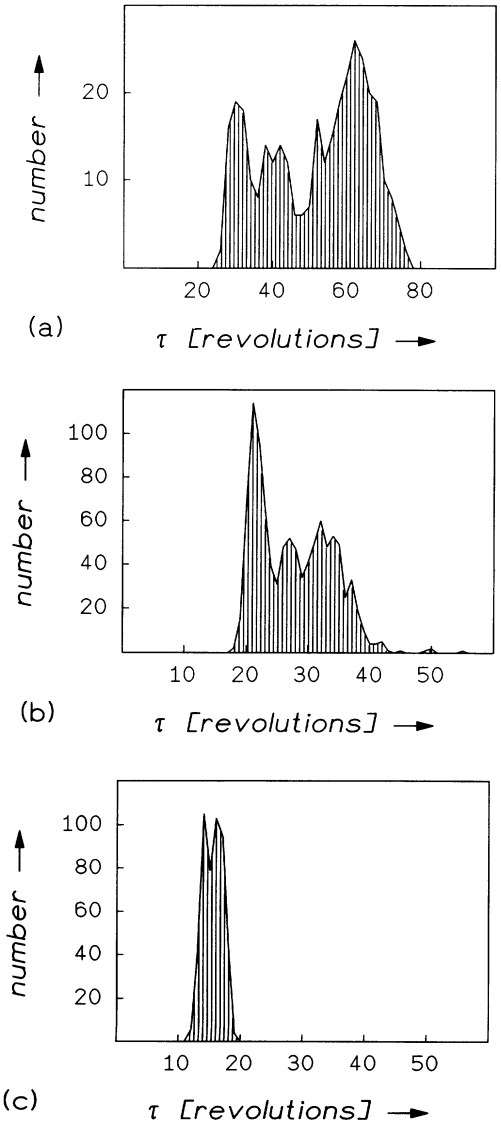

FIG. 9. Histograms of phase lengths obtained at different transverse magnetic field (a) $B=2.67$ mT, (b) $B=2.74$ mT, and (c) $B=3.14$ mT. The constant parameters are the same as in Fig. 5.

Now, we regard the distribution of reinjections already presented in Figs. 8(b) and 8(c). For determining that probability, the first oscillation maxima of the laminar phases located in region B were evaluated. Both the vertical axis of the reinjection histograms as well as that of the return maps have the same scale. Thus we are able to demonstrate that the vertical structures in the middle left part of the maps are points of reinjection into the laminar channel. The histograms make clear that there are only reinjections into the lower part of the channel; i.e., nearly all iterations have to pass the bottleneck. Finally, we emphasize the similar shape of the histograms. That means that the reinjection mechanism is hardly affected under variation of the control parameter.

Figure 9 gives three representative histograms of the laminar phase lengths, obtained for increasing the magnetic-field control parameter. Each histogram is estimated from more than 400 laminar phases. The length of a phase was again measured in number of revolutions. All three histograms display a pronounced upper bound for the laminar phase lengths [at about 80, 40, and 20 revolutions in Figs. 9(a), 9(b), and 9(c), respectively]. This cutoff at the right-hand side of the histograms is characteristic of type-I intermittency. It originates from a minimum channel width being larger than zero, for positive values of the bifurcation parameter.[26] However, the histograms show also a cutoff at their left-hand side [at about 20, 15, and 10 revolutions in Figs. 9(a), 9(b), and 9(c), respectively]. Thus no shorter laminar phases were observed. Furthermore, we point out that the histogram develops an internal structure, ending up with at least two different peaks. The separation between the outermost peaks of a histogram decreases with increasing distance of the control parameter from its critical value at the bifurcation point (see Fig. 9). On the whole, the histograms are in remarkable contrast to the U-shaped distribution of phase lengths proposed for type-I intermittency.[28] An explanation for the shape of the histograms will be one subject of the following discussion.

V. DISCUSSION

We have found strong evidence that the observed transition can be regarded as type-I intermittency in the Pomeau-Manneville classification scheme. However, we recall three facts which seem to be not consistent with preconditions and results of this model of intermittency: First, there were small modulations of the oscillation maxima in Fig. 5(a). Second, the prevailing reinjections are not uniformly distributed along the whole length of the laminar channel, as assumed in general. Third, the histograms of the laminar phase lengths display an un-

familiar shape. It will be the aim of the following to demonstrate that these three departures can, nevertheless, be understood in the frame of the Pomeau-Manneville model of type-I intermittency. We only have to apply slight modifications.

Let us begin with looking at the influence of the measured distribution of reinjections on the shape of the histogram of phase lengths. To this purpose, we have performed a second-order polynomial fit, in order to obtain a functional description of the laminar channel of the return map shown in Fig. 8(b). We then iterate the fitted map. On the one hand, we assume a uniform distribution of reinjections in the whole length of the channel. On the other hand, we take the reinjection points obtained from the measurement. In the former case, one ends up with a U-shaped histogram as proposed by Hirsch, Huberman, and Scalapino.[28] In Fig. 10 this histogram is hatched with ascending lines. The iterations starting in the lower part of the channel have to pass the bottleneck and give rise to the long laminar phases, whereas reinjections above the bottleneck generate the short phases. There are only few reinjections that hit the bottleneck. Thus the histogram exposes a minimum at the intermediate length of phases. In the latter case, the measured reinjection points are solely located before the bottleneck, as shown in Fig. 8(b). Inserting these points into the fitted channel, the histogram only consists of the peak due to long phase lengths. This peak is located on the right-hand side of Fig. 10 (hatched with descending lines).

Next, we compare the singly peaked histogram of Fig. 10 with the more complex histogram of Fig. 9(a). The first was obtained from the simulation based on the measured reinjection probability, while the second in the whole stems from experimental data. It was gained from the time series which we have used to estimate the reinjection points and the return map in Fig. 8(b). Instead of a histogram with only one sharp peak in the vicinity of the mean phase length, we recognize at least two peaks at the left- and right-hand sides of a broader distribution.

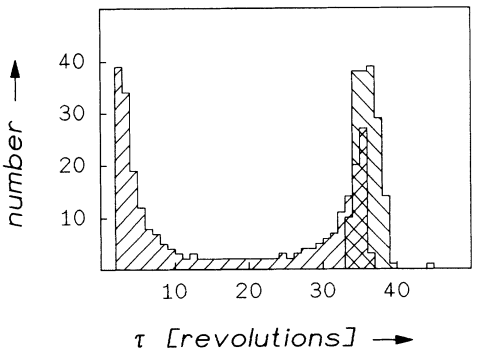

FIG. 10. Histograms of phase lengths obtained from iterating a polynomial fitted to the return map of Fig. 8(b). Using uniformly distributed reinjection points over the whole length of the laminar channel results in a U-shaped histogram (hatched with ascending lines). Inserting the measured reinjection points situated well below the channel leads to a singly peaked histogram (hatched with descending lines).

For solving that discrepancy, the amplitude modulation of the oscillation already indicated in Fig. 5(a) comes to the rescue.

The amplitude modulation can be recognized also in the return map of Fig. 8(a). Instead of an exact (stable) fixed point on the first bisectrix, there is a long roll. Moreover, the return maps of parts (b) and (c) are blurred as a consequence of the modulation. The existence of a torus prior to the saddle-node bifurcation can be deduced from the periodicity of the autocorrelation function of the oscillation maxima plotted in Fig. 11. Moreover, the two frequencies involved are clearly distinguished in the corresponding power spectrum (not shown here), even though the amplitude of the lower-frequency (i.e., the modulation frequency) component is small compared to that of the higher-frequency (i.e., the fundamental frequency) component according to the situation of the time series given in Fig. 5(a). Obviously, the autocorrelation function of the oscillation maxima turns out to represent the most sensitive method. An explanation of the measured histograms can be achieved by the Pomeau-Manneville model via introducing a periodically modulated bifurcation parameter in Eq. (1). For convenience, we assume a sinusoidal modulation[29]

$$\varepsilon=\varepsilon_0+\varepsilon_1\sin(\omega t)\ . \tag{2}$$

For suitably chosen parameter values ε_0 and ε_1, the long roll of data points in Fig. 8(a) derives from the up and down motion of the intersection of the first bisectrix with the parabola given by Eqs. (1) and (2). Next, we apply that model for obtaining a qualitative understanding of the unfamiliar shape of the histograms in Fig. 9. ε_0 is now taken to prevent any point of intersection with the first bisectrix. The upper- and lowermost positions of the resulting parabola are given by the solid curves in the scheme of Fig. 12. The dotted line indicates the mean value the parabola is oscillating around. Note that the parabola stays most of the time at the upper and lower positions. In case of the sinusoidal parameter modulation assumed, the probability for the parabola to stay in a cer-

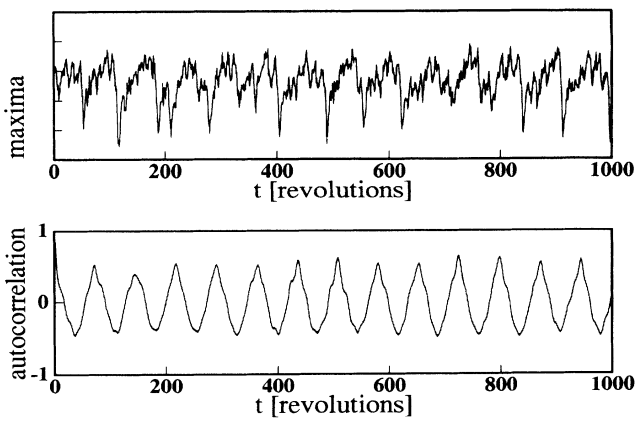

FIG. 11. Time sequence of the oscillation maxima (top) and the corresponding autocorrelation function (bottom) obtained from time series of Fig. 5(a).

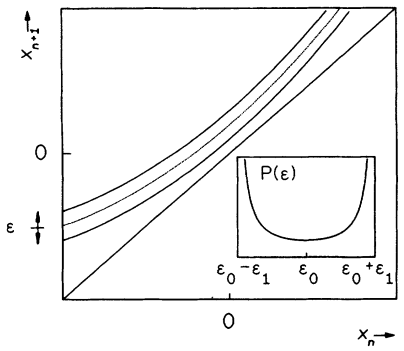

FIG. 12. Sketch of the next amplitude map [Eq. (1)] with periodically modulated bifurcation parameter [Eq. (2)]. The maximum and minimum elongations of the parabola (solid curves) as well as its offset position (dotted curve) are shown. The inset displays the probability density of the bifurcation parameter ε, described by the secans function.

tain position is given by the secans function (see inset of Fig. 12). For a modulation period much larger than the phase length, the parabola and, hence, the channel width will approximately remain constant during one laminar phase. That is, the relatively slow dynamics of the oscillating parabola and the faster dynamics of the iterations inside the laminar channel do not interfere. Consequently, the two peaks of the secans function are to be found in the phase length histogram: The left peak at short phase lengths corresponds to the upper position of the parabola, while the right peak represents the lower position. The histogram presented in Fig. 9(c) approaches the situation reported. It has been measured at short phase lengths for a control parameter value far away from that of the bifurcation point. The histogram already aims to two peaks and, thus, corroborates the model of Eqs. (1) and (2).

Further conclusions concerning the control parameter dependence of the histogram profile can be extracted from the model. Hereto, we decrease the parameter offset ε_0, but fix the modulation amplitude ε_1 and frequency ω. Both the maximum and minimum widths of the channel decrease, whereas their ratio increases. Consequently, the distance between the outer peaks in the histogram becomes larger, as measured in Figs. 9(a) and 9(b). The appearance of interior peaks may result from the fact that our assumption we have started with (modulation period of the bifurcation parameter much longer than the laminar phase) is no longer valid. We just have to take into account that, in the vicinity of the bifurcation point, the channel width undergoes several oscillatory cycles during one laminar phase. Preliminary numerical simulations have pointed out that the interior peaks of the histograms can be reproduced in the parameter range near the bifurcation point.

VI. CONCLUSION

To summarize, we have shown that type-I intermittency takes place during impact ionization breakdown in extrinsic germanium. Via analyzing the proper scaling behavior of the mean laminar phase length, we provide strong evidence that a saddle-node bifurcation governs the system dynamics. Small modulation of the oscillation amplitudes gives first hints that the present type of intermittency does not start from a limit cycle, but from a torus. Departures from the expected U-shaped distribution of the laminar phase lengths are demonstrated to originate both from a narrow, nonuniform reinjection probability of the embedding chaotic attractor and from a toroidal dynamics of the laminar phases. The concrete form of the distribution of phase lengths can be modeled by the help of a periodically modulated bifurcation parameter.

ACKNOWLEDGMENTS

The authors wish to thank G. Baier, T. Buzug, W. Clauss, H. Herzel, M. Hirsch, R. P. Huebener, G. Hüpper, M. Klein, U. Rau, A. Rein, O. E. Rössler, E. Schöll, and R. Stoop for helpful discussions. This work was supported by a grant of the Volkswagen-Stiftung.

[1]B. B. Mandelbrot, *Fractals from Chance and Dimension* (Freeman, San Francisco, 1977).
[2]D. J. Tritton, *Physical Fluids Dynamics* (Van Nostrand-Reinhold, New York, 1977).
[3]P. Manneville and Y. Pomeau, Phys. Lett. **75A**, 1 (1979); Physica D **1**, 219 (1980); Y. Pomeau and P. Manneville, Commun. Math. Phys. **74**, 189 (1980).
[4]C. Grebogi, E. Ott, F. Romeiras, and J. A. Yorke, Phys. Rev. A **36**, 5365 (1987).
[5]F. T. Arecchi, R. Badii, and A. Politi, Phys. Lett. **103A**, 3 (1984).
[6]J. D. Keeler and J. D. Farmer, Physica D **23**, 413 (1986).
[7]Y. Pomeau, J. C. Roux, A. Rossi, S. Bachelart, and C. Vidal, J. Phys. (Paris) **42**, L-271 (1981); T. Mullin and G. Darbyshire, Europhys. Lett. **9**, 669 (1989).
[8]J. Y. Huang and J. J. Kim, Phys. Rev. A **36**, 1495 (1987); H. Herzel, P. Plath, and P. Svensson, Physica D **48**, 340 (1991).
[9]M. Dubois, M. A. Rubio, and P. Berge, Phys. Rev. Lett. **51**, 144 (1981); G. Baier, K. Wegmann, and J. L. Hudson, Phys. Lett. A **141**, 340 (1989); N. Kreisberg, W. D. McCormick, and H. L. Swinney, Physica D **50**, 463 (1991).
[10]W. J. Yeh and Y. H. Kao, Appl. Phys. Lett. **42**, 229 (1983).
[11]C. Jeffries and J. Perez, Phys. Rev. A **26**, 2117 (1982); R. W. Rollins and E. R. Hunt, *ibid.* **29**, 3327 (1984).
[12]T. J. Price and T. Mullin, Physica D **48**, 29 (1991).
[13]J. Peinke, U. Rau, W. Clauss, R. Richter, and J. Parisi, Europhys. Lett. **9**, 743 (1989).
[14]R. Richter, J. Peinke, W. Clauss, U. Rau, and J. Parisi, Europhys. Lett. **14**, 1 (1991).
[15]J. Parisi, U. Rau, J. Peinke, and K. M. Mayer, Z. Phys. B **72**,

225 (1988).
[16]E. Schöll, *Nonequilibrium Phase Transitions in Semiconductors* (Springer, Berlin, 1987).
[17]J. Peinke, W. Clauss, R. P. Huebener, A. Kittel, J. Parisi, U. Rau, and R. Richter, in *Spontaneous Formation of Space-Time Structures and Criticality,* edited by T. Riste and D. Sherrington (Kluwer, Dordrecht, 1991), p. 145.
[18]J. Peinke, D. B. Schmid, B. Röhricht, and J. Parisi, Z. Phys. B **66**, 65 (1987).
[19]A. Brandl, W. Kröninger, W. Prettl, and G. Obermair, Phys. Rev. Lett. **64**, 212 (1990).
[20]J. Peinke, J. Parisi, B. Röhricht, K. M. Mayer, U. Rau, W. Clauss, R. P. Huebener, G. Jungwirt, and W. Prettl, Appl. Phys. A **48**, 155 (1989), and references therein.
[21]W. Clauss, U. Rau, J. Parisi, J. Peinke, R. P. Huebener, H. Leier, and A. Forchel, J. Appl. Phys. **67**, 2980 (1990).
[22]K. M. Mayer, J. Parisi, U. Rau, J. Peinke, and R. P. Huebener, Solid State Commun. **73**, 369 (1990).
[23]K. M. Mayer, J. Parisi, and R. P. Huebener, Z. Phys B **71**, 171 (1988).
[24]K. M. Mayer, J. Parisi, J. Peinke, and R. P. Huebener, Physica D **32**, 306 (1988).
[25]G. Hüpper and E. Schöll, Phys. Rev. Lett. **66**, 2372 (1991).
[26]P. Berge, Y. Pomeau, and C. Vidal, *Order within Chaos* (Hermann, Paris, 1984).
[27]F. T. Arecchi, A. Lapucci, R. Meucci, J. A. Roversi, and P. H. Coullet, Europhys. Lett. **6**, 677 (1988).
[28]J. E. Hirsch, B. A. Huberman, and D. J. Scalapino, Phys. Rev. A **25**, 519 (1982).
[29]H. Daido, Prog. Theor. Phys. (Kyoto) **70**, 879 (1983); **71**, 402 (1984).

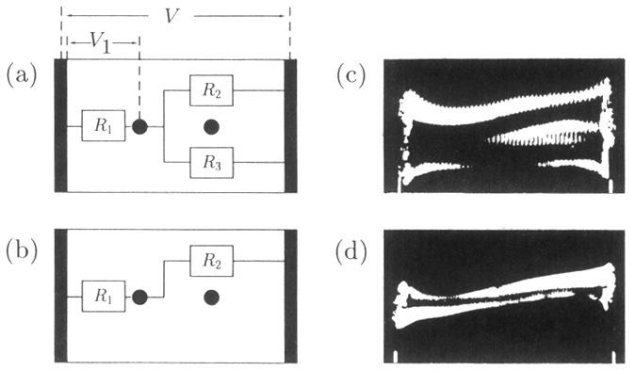

FIG. 4. (a),(b) Circuitry schemes and (c),(d) measured images of two filamentary structures: (a),(c) a Y-shaped and (b),(d) a single current filament. The images (c) and (d) are obtained from a different sample (of about 0.5 mm length) via use of low-temperature scanning electron microscopy (for details, see Refs. 23 and 24).